

HIGHER-MODE EFFECTS IN GLASS PANE RESPONSE TO CLOSE-RANGE BLAST: A FINITE ELEMENT AND SDOF MODEL COMPARISON

Ilham Nurhuda¹, Nelson T.K. Lam²

¹ Diponegoro University, Semarang, INDONESIA

² The University of Melbourne, Melbourne, AUSTRALIA

Abstract: The structural performance of glass panes under blast-induced pressures is commonly analyzed using single-degree-of-freedom (SDOF) models, which assume that the response is governed by the fundamental mode of vibration. However, in close-range explosion scenarios where the load duration is significantly shorter than the natural period of the glass pane, higher-mode effects can become significant. To enhance the blast resistance of glass panels, it is important to understand their behavior under a wide range of explosion scenarios, including close-range blasts. Unlike previous studies that have primarily focused on long-distance explosions with relatively long load durations, this study investigates the dynamic response of glass panes under short-duration blast loads. The investigation is conducted using calibrated finite element (FE) simulations on glass panes with varying dimensions and thicknesses, subjected to different blast intensities. Key response parameters examined include deflection shapes, bending stresses, and shear stresses. Results indicate that while the SDOF model can reasonably predict the maximum deflection of glass panes, it significantly underestimates peak bending and shear stresses in short-duration blast scenarios. A power-law relationship is proposed to quantify the discrepancy between SDOF and FE stress predictions as a function of the load duration-to-natural period ratio. These findings reveal the limitations of conventional SDOF models and highlight the need to account for higher-mode effects in the design of glazing systems exposed to close-in explosions.

Keywords: glass pane, close-range explosion, finite element, SDOF, higher modes

ВЛИЯНИЕ ВЫСШИХ ФОРМ КОЛЕБАНИЙ НА ОТКЛИК СТЕКЛЯННЫХ ПАНЕЛЕЙ ПРИ БЛИЖНИХ ВЗРЫВАХ: СРАВНЕНИЕ МОДЕЛЕЙ МКЭ И SDOF

Ильхам Нурхуда¹, Нельсон Т.К. Лам²

¹ Университет Дипонегоро, Семаранг, ИНДОНЕЗИЯ

² Мельбурнский университет, Мельбурн, АВСТРАЛИЯ

Аннотация: Поведение стеклянных панелей при взрывных воздействиях обычно описывается моделями SDOF, основанными на фундаментальной форме колебаний. Однако при ближних взрывах с короткой длительностью импульса значимыми становятся высшие формы. В работе с использованием метода конечных элементов исследован динамический отклик панелей различной толщины и размеров при кратковременных нагрузках. Рассмотрены прогибы, изгибные и касательные напряжения. Показано, что модель SDOF удовлетворительно предсказывает максимальный прогиб, но существенно занижает пиковые напряжения. Для оценки расхождений предложена степенная зависимость от отношения длительности импульса к собственному периоду колебаний. Результаты выявляют ограничения классических моделей SDOF и необходимость учёта высших форм при проектировании остекления, подверженного ближним взрывам.

Ключевые слова: стеклянная панель, ближний взрыв, метод конечных элементов, модель SDOF, высшие формы колебаний

1. INTRODUCTION

Buildings such as government offices, hotels, and commercial facilities are often potential targets of terrorist attacks. These types of structures frequently incorporate large glass panes in their façades, which are widely recognized as the most vulnerable components during an explosion [1], [2]. Evidence from past terrorist incidents shows that buildings designed in accordance with modern codes of practice generally experienced limited structural damage. However, extensive damage to surrounding glass façades was frequently observed. Flying glass fragments from shattered panes have been identified as one of the primary causes of injury [3], [4].

The behaviour of glass panes subjected to explosions can be analysed numerically using the finite element method (FEM), as demonstrated in previous studies [5], [6]. However, FEM analyses typically require considerable time and computational resources for both modelling and simulation. Therefore, for practical purposes, simplified single-degree-of-freedom (SDOF) models are often used as an alternative [7], [8], [9], [5]. Given that blast pressures generated by long-distance explosions generally have longer durations than those from close-range blasts, the response of the glass pane in such cases is often dominated by the fundamental mode of vibration. As a result, SDOF models can be effectively employed to estimate the response of glass panes under long-duration blast loading, offering a more practical alternative to complex numerical simulations.

Long distance explosion scenarios are generally valid in situations where security measures have precluded the possibility of a large explosion (generated by a car bomb or truck bomb, for example) to be detonated at close range to a protected target. However, the target, or part of it, could still be susceptible to attacks by the use of smaller explosion devices at close range. Examples of such “minor” blast scenarios include the parcel bomb incident in Paris in 2007 and the grenade attack on the US embassy in

Greece in the same year. This paper focuses on the dynamic behaviour of glass panes when subject to close-range explosions in which blast pressures of much shorter duration and higher peak overpressure are generated. With load duration shorter than that of the fundamental natural period of glass panes, higher modes effects can become significant and need to be taken into account in the strength evaluation.

This paper investigates the influence of higher vibration modes on the dynamic response of glass panes. The response parameters of interest include displacement, normal (bending) stress, and transverse shear stress within the glass panes. The main contributions of this paper are as follows: (1) validation of finite element (FE) modeling under short-duration loading; (2) a comparative analysis of the responses obtained from calibrated FE simulations and SDOF models across varying ratios of load duration (td) to the natural period (T) of the glass panes; and (3) derivation of correction formulae for SDOF stress estimates under higher-mode influence.

2. METHODOLOGY

2.1. Geometry of Glass Panes

This study examines the behavior of glass panes supported on two opposite sides, a configuration commonly found in façade walls, interior partitions, and display windows. This type of support typically results in a relatively long fundamental natural period compared to the duration of a blast load.

Table 1. Dimension of glass panes

Pane Dimensions (mm)	Glass Thickness (mm)
500 x 500	4
1000 x 1000	10
1000 x 1000	4
2000 x 2000	19

The glass panes were analyzed in three size categories: small (500 mm x 500 mm), medium (1000 mm x 1000 mm), and large (2000 mm x 2000 mm). The thickness of each pane was

selected to meet wind load requirements in accordance with the AS 1288 standard [10], ensuring structural adequacy under normal service conditions. The detailed pane dimensions and thicknesses are listed in Table 1.

2.2. Finite Element (FE) Modelling and Verification

In this study, the dynamic behaviour of the glass panes was studied analytically using LS-DYNA, an explicit, non-linear 3D finite element analysis (FEA) code [11]. The glass panes were modelled using shell elements. Figure 1a shows a finite element (FE) model of a glass pane supported on 2 sides. The X, Y, and Z axes in Figure 1a are the global axes in the FE model which are used as a reference for calculating the distribution of blast pressure and internal forces in the glass pane. Point O denotes the centre of the pane, while Point A is located at the support such that line OA is parallel to the X-axis. Figure 1b shows a typical shell element. Notations r , s , and t in Figure 1b refer to local axes in a shell element, and a_k denotes the element thickness at node k . The shell elements used in this analysis considered both large deformation and transverse shear in the elements [12], [11], [13]. Annealed glass was used throughout the study. The glass material was modelled as a linearly elastic isotropic material with Young’s modulus =

68,500 MPa, Poisson’s ratio = 0.23 and density = 2,500 kg/m³.

The analysis procedure was verified against results from physical experiments. Physical tests were conducted on a glass pane of size 1000 mm x 1000 mm x 5 mm, which was simply supported along two parallel edges. The glass pane was subject to an impact load from an elastic ball with a diameter of 27 mm. The elastic ball was dropped from a height of 1400 mm onto the centre of the pane. An accelerometer was attached to the ball to record its acceleration during impact. The deflection of the glass pane was measured using linear variable displacement transducers (LVDTs) positioned beneath the glass. The test set-up is illustrated in Figure 2.

The impact load, illustrated in Figure 3, was calculated by multiplying the measured acceleration by the combined mass of the elastic ball and the attached accelerometer. The duration of the impact loading, also shown in Figure 3, was approximately 3 milliseconds, significantly shorter than the fundamental natural period of vibration of the glass pane ($T = 84$ ms). This impact duration is consistent with test results reported in the literature for a single loading cycle (Zhang et al., 2025). Since the load duration was much shorter than the fundamental period, the dynamic response of the glass pane was strongly influenced by higher vibration modes, as evidenced in Figure 4.

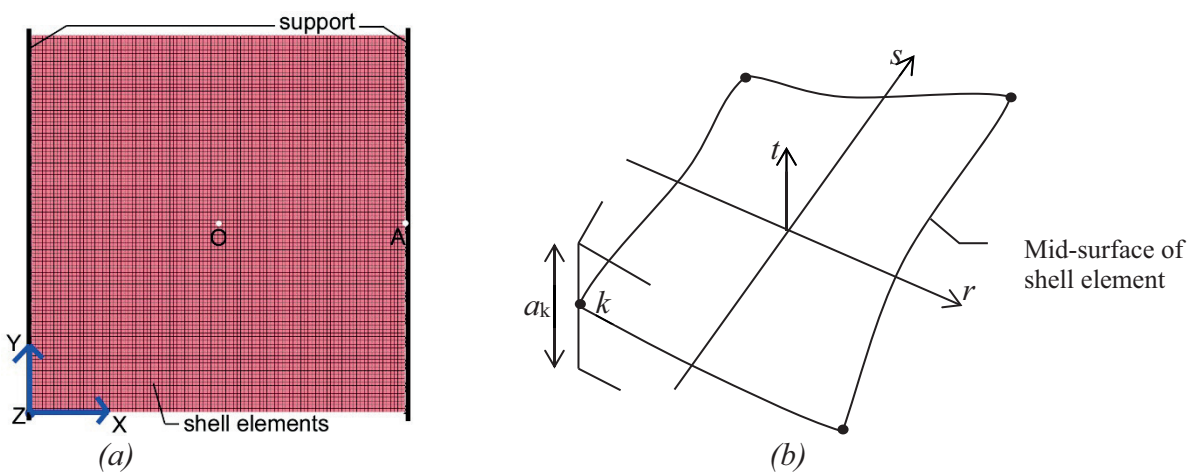


Figure 1. Finite element model (a) FE model for glass panes supported on 2 sides, (b) Shell element [15]

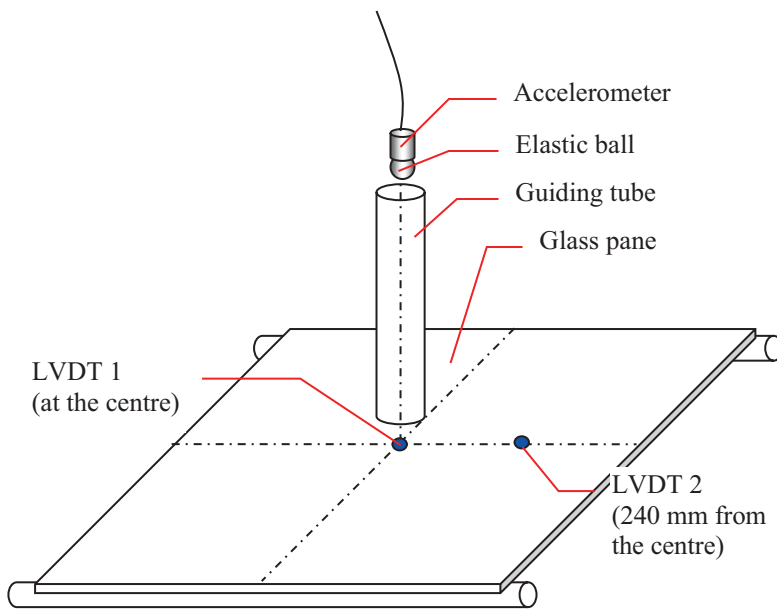


Figure 2. The physical test set up

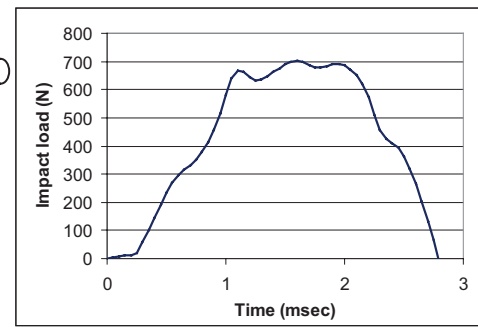
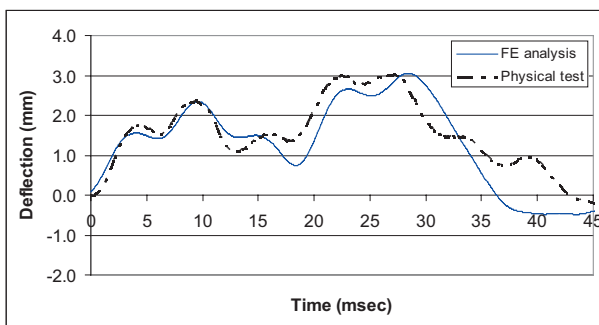
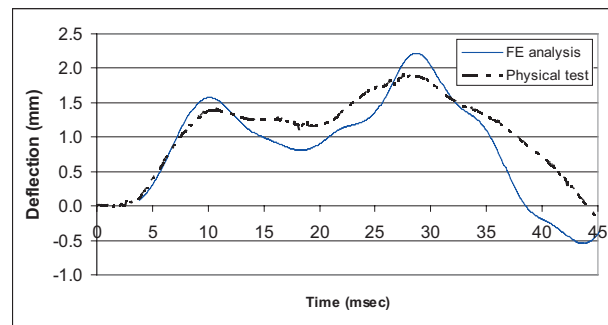


Figure 3. Impact load



(a)



(b)

Figure 4. Deflections of the glass pane (a) at LVDT 1, (b) at LVDT 2 (refer Figure 2)

Figure 4 presents a comparison between deflections obtained from the physical experiment and those predicted by the finite element (FE) analyses. As shown, the FE predictions align well with the experimental observations, particularly during the early phase of the response. However, in the physical test, the glass pane experienced multiple impacts due to the ball bouncing upon contact (Zhang et al., 2025). Since this aspect of the experiment was not incorporated into the FE model, the numerical predictions could not fully match the measured deflections throughout the entire response. Nevertheless, the applicability of the developed FE models for simulating the dynamic behaviour of glass panes has been successfully verified.

2.3. SDOF Model Formulation and Assumptions

Analysis using a representative finite element (FE) model can provide accurate predictions of a structure’s dynamic behaviour. However, such analysis requires sophisticated FE software, such as LS-DYNA. Simpler methods, such as single-degree-of-freedom (SDOF) models, have been widely used to predict structural responses under blast loading. SDOF models have been shown to provide reasonable estimates when the explosion originates from a long distance [7]. However, their applicability to glass panes subjected to close-range explosions remains uncertain and warrants further investigation to evaluate the accuracy of the results obtained from SDOF-based analyses.

In SDOF model analyses, the dynamic properties of the structure are characterized by its equivalent mass (m^*), equivalent stiffness (k^*), and equivalent damping (c) as shown in Figure 5a. The applied loads must also be transformed into an equivalent force. Methods for calculating these SDOF parameters are well documented in the literature [8], [16], [17]. In this study, the SDOF parameters representing the glass pane were calculated using Rayleigh's method, which is based on the principle of conservation of energy. The blast induced pressure was defined by Eq 1, and the deflection shape function of the glass pane was of the sinusoidal form as defined by Eq 2 forming part of the Rayleigh's method. The equivalent mass (m^*) and equivalent stiffness (k^*) representing the glass pane were calculated according to the deflection shape function using Eqs 3 – 6. Once these parameters were obtained, the fundamental natural period of vibration of the glass pane (T) could be estimated.

$$p(x, y, t) = pr(t) \cdot \left[\frac{R^2}{\left(x - \frac{a}{2}\right)^2 + \left(y - \frac{b}{2}\right)^2 + R^2} \right] + pi(t) \left[1 - \frac{R}{\sqrt{\left(x - \frac{a}{2}\right)^2 + \left(y - \frac{b}{2}\right)^2 + R^2}} \right]^2 \quad (1)$$

$$\psi(x, y) = \sin \frac{\pi x}{a} \quad (2)$$

for plates supported on 2 parallel sides

$$\psi(x, y) = \sin \frac{\pi x}{a} \sin \frac{\pi y}{b}$$

for plates supported on 4 sides

$$m^* = \int_0^a \int_0^b m \cdot \psi(x, y)^2 dx \cdot dy \quad (3)$$

$$k^* = D \int_0^a \int_0^b \left\{ -2(1 - \nu) \cdot t \right\} dx dy \quad (4)$$

$$s = \left[\frac{\partial^2 \psi(x, y)}{\partial x^2} + \frac{\partial^2 \psi(x, y)}{\partial y^2} \right]^2$$

$$t = \left[\frac{\partial^2 \psi(x, y)}{\partial x^2} \frac{\partial^2 \psi(x, y)}{\partial y^2} - \left(\frac{\partial^2 \psi(x, y)}{\partial x \partial y} \right)^2 \right]$$

$$D = Eh^3 / 12(1 - \nu^2) \quad (5)$$

$$p^*(t) = \int_0^a \int_0^b p(x, y, t) \cdot \psi(x, y) dx \cdot dy \quad (6)$$

where $\psi(x, y)$ is the deflection shape function, p^* is the equivalent force, x and y are coordinates on the glass pane measured from the bottom left corner of the pane (see Figure 1a), a and b are the width and length of the pane, h is the thickness, t is time, $p(x, y, t)$ is the blast pressure function, $pr(t)$ is the reflected pressure at time t , $pi(t)$ is the incident pressure at time t , R is the distance from the explosive to the centre of the target, m is mass per unit area, E is Young's modulus, and ν is Poisson's ratio.

For glass panes supported on all four sides, membrane action has been found to dominate under large deflections [17]. An SDOF model that incorporates the contribution of membrane stiffness is shown in Figure 5b, and its equation of motion is presented in Equation 7. The displacement $x(t)$ in Equation 7 can be solved numerically using the Central Difference Method for step-by-step time integration.

$$m^* \ddot{x}(t) + c \cdot \dot{x}(t) + k^* \cdot x(t) = p^*(t) \quad (7)$$

where $x(t)$, $\dot{x}(t)$, and $\ddot{x}(t)$ are the displacement, velocity, and acceleration at the centre of glass plates, and c is damping coefficient.

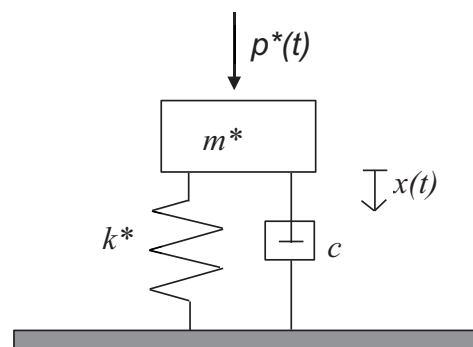


Figure 5. SDOF model

2.4. Blast Loading Model and Scenarios

Blast pressures result from the instantaneous release of energy during explosive detonation. The magnitude of the blast loading is typically quantified in terms of the equivalent TNT weight

of the explosive [18], [4], [19], [2]. For explosives other than TNT, their weight can be converted into an equivalent TNT weight using Equation 8 [19].

$$W_{TNT} = W_{EXP} \cdot (Q_{EXP} / Q_{TNT}) \quad (8)$$

where W_{TNT} is the equivalent TNT charge weight, W_{EXP} is the weight of the explosive, Q_{EXP} is the mass specific energy of the detonated explosive, and Q_{TNT} is the mass specific energy of TNT.

An explosion produces hot gases that expand rapidly, displacing the surrounding air and generating blast waves in the atmosphere. As the blast wavefront reaches the ground, it is reflected, and the interaction between the incident and reflected waves results in even higher pressures. When the blast wave strikes a target, its expansion is constrained, causing a sudden rise in pressure on the target surface, as illustrated in Figure 6.

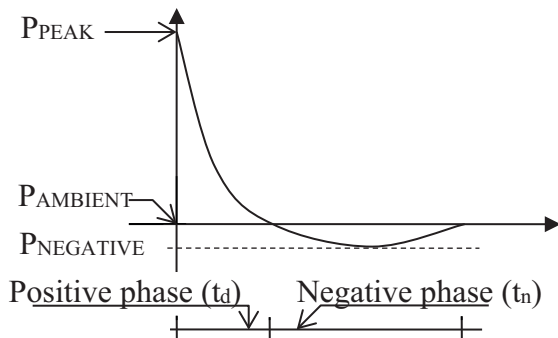


Figure 6. Typical pressure-time history

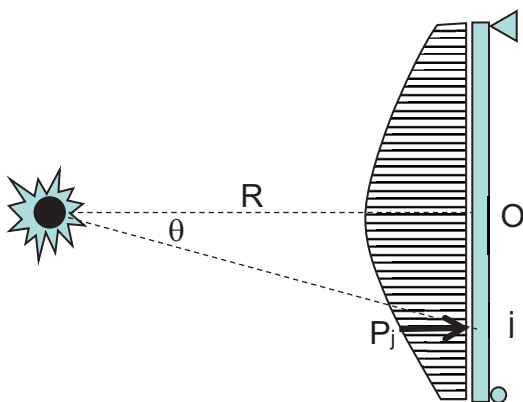


Figure 7. Distribution of blast pressure

The blast-induced pressure then gradually decreases to ambient levels at time t_d , marking the end of the positive phase. Following this, the pressure may drop below ambient, creating a negative (suction) phase, before returning to normal atmospheric conditions. Since the negative phase typically reduces the target's deflection, its effect can be neglected, as is done in this study.

The blast pressure parameters illustrated in Figure 6 depend on various factors, including charge weight (expressed as equivalent TNT weight), stand-off distance, the location of the detonation (in air or on the surface), and the presence of obstacles between the explosive and the target. Methods for estimating blast pressure–time histories are well-documented in the literature [19]. Existing analytical approaches can generally be grouped into two main categories: (1) analytical methods that use empirical formulae and charts, and (2) numerical simulations, such as computational fluid dynamics (CFD), which are computationally expensive and thus better suited for modelling blast effects on structures with complex geometries or in complicated environments [20], [21]. Blast scenarios involving structures with regular geometry in standard environments, analytical methods based on formulae and graphs are typically sufficient [13], [19].

In this study, the ConWep method [22] was used to model the blast-induced pressures on the glass panes. ConWep is based on empirical test data and analytical approximations, and has been widely adopted by both researchers and practitioners. Furthermore, it has been shown to provide reliable predictions of blast effects [23]. The distribution of blast-induced pressure on the surface of a target is significantly influenced by the stand-off distance. At long stand-off distances, the distance from the explosive charge to any point on the planar target is nearly uniform, resulting in a small angle of incidence (θ), as illustrated in Figure 7. Under such conditions, the blast pressure can be reasonably assumed to be uniformly distributed across the target surface. However, at short stand-off distances, this

uniform pressure assumption is no longer valid due to the increased variation in angle and distance. In this study, the distribution of the

blast load, $P_j(t)$, on the glass panes is calculated using Equation 9 [24].

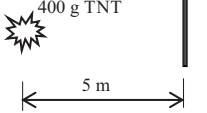
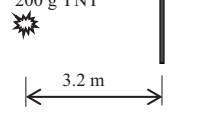
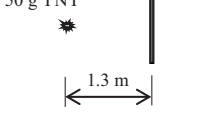
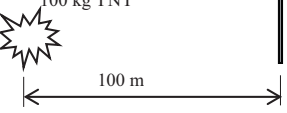
	Scenario A	Scenario B	Scenario C	Scenario D
				
P_i	26.51 kPa	37.48 kPa	79.81 kPa	5.53 kPa
P_r	58.57 kPa	85.77 kPa	208.4 kPa	11.27 kPa
td	3.1 ms	2.284 ms	1.188 ms	28.12 ms
Glass Panes	500 mm x 500 mm x 4 mm ($td/T = 0.12$)	1000 mm x 1000 mm x 4 mm ($td/T = 0.02$)	2000 mm x 2000 mm x 19 mm ($td/T = 0.01$)	2000 mm x 2000 mm x 19 mm ($td/T = 0.32$)
		1000 mm x 1000 mm x 10 mm ($td/T = 0.05$)		

Figure 8. Blast scenarios

$P_j(t) = Pr_o(t) \cdot \cos^2(\theta) + Pi_o(t) \cdot (1 - \cos(\theta))^2$ (9) where $Pr_o(t)$ and $Pi_o(t)$ are the reflected and incident pressures respectively at point “O” as defined by ConWep, and θ is the angle of incidence as illustrated in Figure 7.

This investigation focused on analysing the effects of explosions generated by handheld bombs, such as grenades and parcel bombs, at close range to the target. The equivalent TNT weights in these scenarios ranged from 50 to 400 grams. In this study, explosives were positioned directly in front of the centre of the glass panes at four different stand-off distances: 1.3 m, 3.2 m, 5.0 m, and 100 m. Details of the blast scenarios are presented in Figure 8. Scenario D represents a case where a glass pane responds to a long-range explosion at a stand-off distance of 100 m, included for comparison purposes.

3. RESULTS AND DISCUSSIONS

3.1. Deflection of Glass Panes

Figure 9a presents the displacement-time history at the centre of a glass pane measuring 500 mm x 500 mm x 4 mm, subjected to blast-induced pressure with a duration of 3.1 ms (scenario A) or corresponding to a td/T ratio of 0.12. Figure 9b presents results for a glass pane of size 1000 mm x 1000 mm x 10 mm under a blast pressure

duration of 2.3 ms (scenario B), or $td/T = 0.05$. Figures 9c and 9d present results of glass panes of identical size (2000 mm x 2000 mm x 19 mm) but subjected to different blast scenarios. The glass pane in Figure 9c was exposed to a close-range explosion, while the one in Figure 9d experienced a long-range explosion. Across Figures 9a – 9d, it is consistently observed that a decrease in the td/T ratio increases the contributions of higher modes, as indicated by the wavy broken lines in the figures.

Results from the finite element (FE) analysis are presented alongside predictions from the SDOF models in Figures 9a–9d. The SDOF model used in the analyses did not include membrane stiffness (Figure 4a). Figures 9a–9d demonstrate that the deflection profiles obtained from the SDOF model without accounting for higher-mode effects can still be representative of the actual behaviour, particularly when the td/T ratio is not less than 0.05. However, when the td/T ratio becomes smaller (as shown in Figure 9c), the accuracy of the SDOF model predictions may diminish. Furthermore, Figure 9c illustrates that higher-mode effects can lead to noticeable reduction in the maximum deflection of the glass pane.

Since the parameters defining the SDOF generalization are based on an assumed deflection shape, it is important to compare this

assumed sinusoidal function with deflection profiles obtained from finite element (FE) analyses. Figure 10a shows the normalized deflection shape of the glass pane, as computed

from the FE analysis (along the OA section defined in Figure 1a) at the moment of maximum deflection.

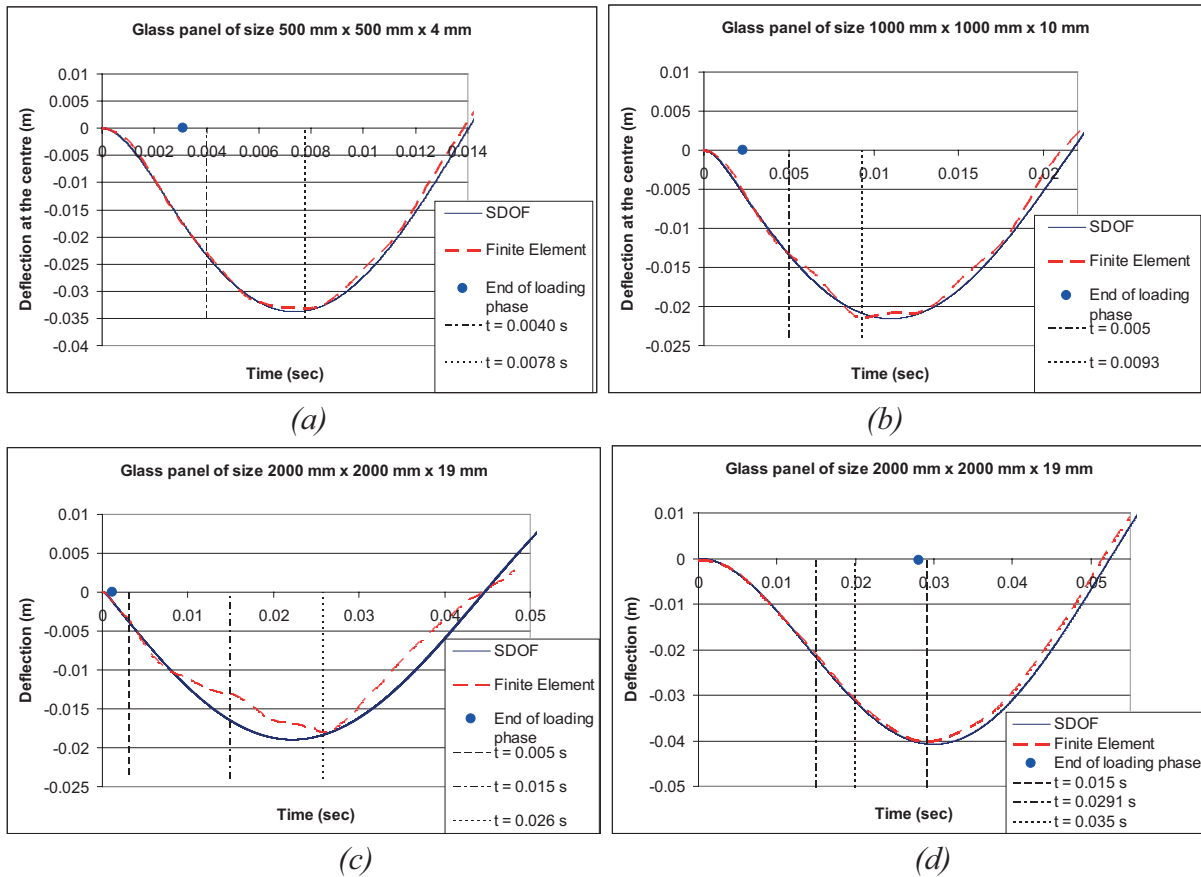


Figure 9. Deflection-time history of glass panes (a) $td/T = 0.12$, (b) $td/T = 0.05$, (c) $td/T = 0.01$, (d) $td/T = 0.32$

Figures 10b–10d present deflection shapes at other time instances, as indicated in the respective legends. Overall, the sinusoidal deflection shape assumed in the SDOF generalization shows reasonable agreement with the FE results. However, a noticeable discrepancy is observed in Figure 10c, where the td/T ratio is very small (0.01).

3.2. Bending Stress

The strength of glass is commonly evaluated based on the major principal stresses estimated

on the surface of the glass pane [13], [25], [16], [26]. For glass panes supported on two parallel sides, these stresses are primarily governed by bending. Figures 11a–11c present the time history of the maximum bending stresses at the centre of the glass pane. The results reveal a highly fluctuating time-history of bending stress, in contrast to the more predictable deflection response. This fluctuation is indicative of the significant influence of higher vibration modes on the bending stress.

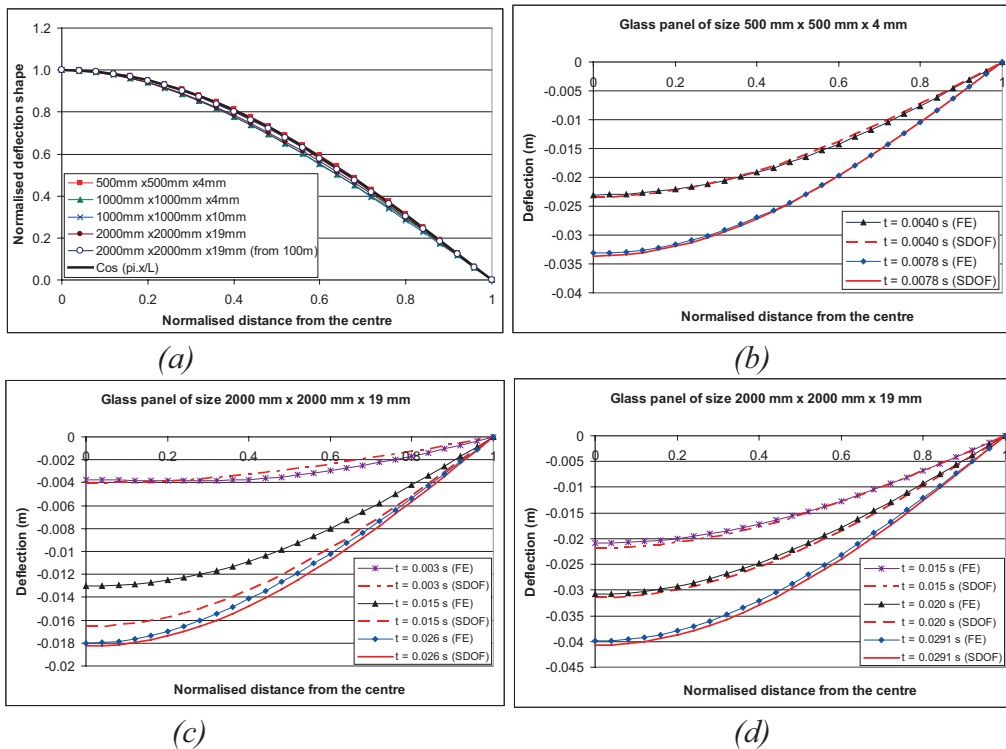


Figure 10. Deflection shape along section OA (a) Maximum deflection shape for different glass panes (b) 500 mm x 500 mm x 4 mm glass pane ($td/T = 0.12$), (c) 2000 mm x 2000 mm x 19 mm glass pane ($td/T = 0.01$), (d) 2000 mm x 2000 mm x 19 mm glass pane ($td/T = 0.32$)

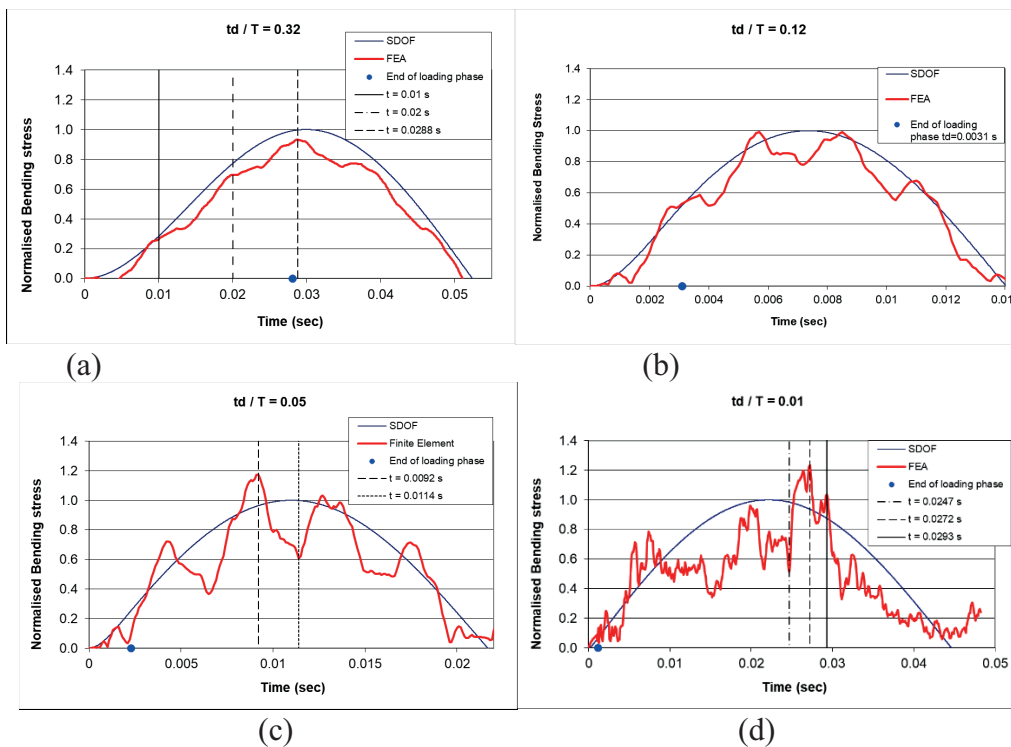


Figure 11. Time history of the normalized bending stress at the centre of (a) a glass pane measuring 2000 mm x 2000 mm x 19 mm, with $td/T=0.32$, (b) a glass pane measuring 500 mm x 500 mm x 4 mm, with $td/T=0.12$; (c) a glass pane measuring 1000 mm x 1000 mm x 10 mm, with $td/T=0.05$, (d) a glass pane measuring 2000 mm x 2000 mm x 19 mm, with $td/T=0.01$

Figure 11a demonstrates good correlation between the predictions of the generalized SDOF model and those from the finite element (FE) analysis. In blast scenarios with lower td/T ratios (Figures 11b and 11c), the maximum stress values predicted by the generalized SDOF model are significantly lower than those obtained from the FE analysis. While SDOF analysis offers the advantages of simplicity and lower computational cost, some limitations in accuracy have been identified. As shown in Figure 11, the magnitude of stress fluctuations increases as the td/T ratio decreases. Therefore, the accuracy of the SDOF model can be improved by modifying its results to account for higher-mode effects, whose significance has been shown to depend on the td/T ratio. The discrepancy between the FE and SDOF predictions of bending stress can be expressed as the ratio $\sigma_{FEA} / \sigma_{SDOF}$. Figure 12 illustrates that this ratio increases as the td/T ratio decreases. Furthermore, the relationship between σ_{FEA} and σ_{SDOF} can be modelled using the power function presented in Equation 8, which is valid for rectangular glass panes supported on two sides with td/T values ranging between 0.01 and 0.12.

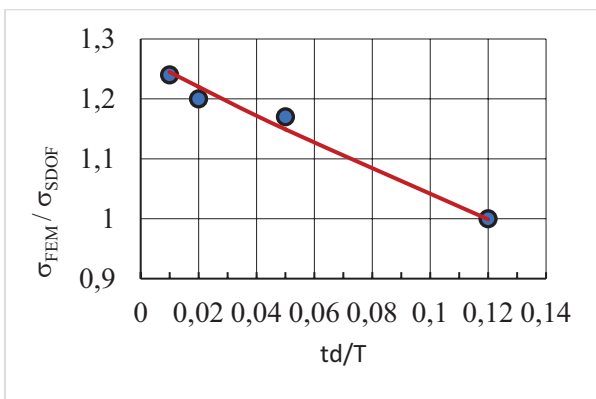
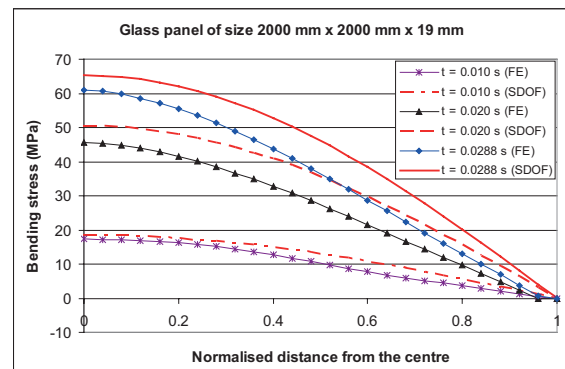


Figure 12. Relationship between $\sigma_{FEA}/\sigma_{SDOF}$ and td/T .

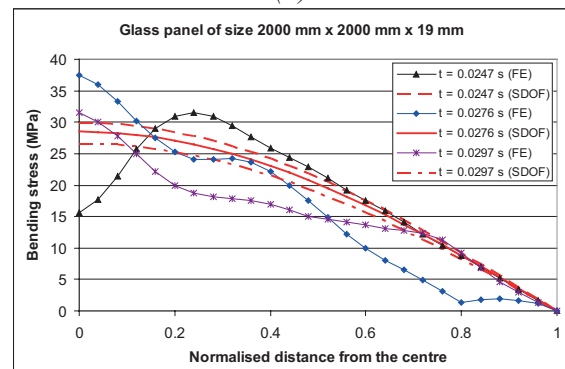
$$\sigma_{FEA} = 1.27 \sigma_{SDOF} \cdot e^{-2(td/T)} \quad (8)$$

The probabilistic strength of glass depends on the effective area of the glass pane, which is influenced by the surface stress distribution [27].

Under dynamic conditions, surface stresses vary over time, as illustrated in Figures 13a–13b, and can be difficult to predict. Discrepancies between estimates from the SDOF analysis and those from the finite element (FE) analysis are particularly pronounced when the td/T ratio is small. Even at $td/T = 0.32$ (Figure 13a), notable differences remain. For glass panes subjected to close-range explosions (i.e., small td/T ratios), the time-dependent variation of surface stress must be considered when calculating the probabilistic strength of the glass. However, detailed considerations of failure probability are beyond the scope of this paper.



(a)



(b)

Figure 13. Maximum bending stress profile along section OA in: (a) glass panes of size 2000 mm x 2000 mm x 19mm ($td/T=0.32$), (b) glass panes of size 2000 mm x 2000 mm x 19mm ($td/T=0.01$)

3.3. Transverse Shear Stress

In glass panes subjected to static loading, the effect of transverse shear stress is often neglected. This is because, under static conditions, the

magnitude of transverse shear stress in thin glass panes is typically much smaller than that of the principal (bending) stresses. However, under dynamic loading, the bending moment stress profile varies with time, and its slope can be significantly steeper than that in static loading. Since transverse shear stress is related to the rate of change of bending moment, its magnitude under dynamic conditions can become substantial. The significance of transverse shear stress in dynamically loaded glass panes is illustrated in Figure 14, where its intensity is expressed as the ratio of maximum transverse shear stress to maximum bending stress ($\tau_{yz_{max}} / \sigma_{b_{max}}$).

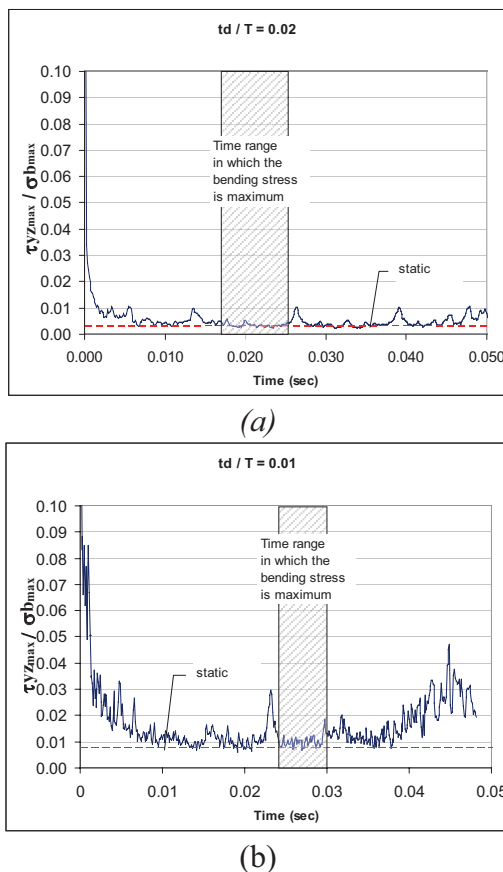


Figure 14. Time history of the ratio of maximum shear stress to the maximum major principal stress (a) in glass pane of size 1000 mm x 1000 mm x 4 mm, (b) in glass pane of size 2000 mm x 2000 mm x 19 mm

Figures 14a and 14b present the time histories of the ratio $\tau_{yz_{max}} / \sigma_{b_{max}}$ for $td/T = 0.02$ and 0.01 , respectively. The shaded regions in both figures

indicate the time intervals during which the bending stress reaches its maximum. During these periods of peak bending stress, the ratio $\tau_{yz_{max}} / \sigma_{b_{max}}$ is generally low and comparable to values observed under static loading conditions. However, the figures also show that the ratio $\tau_{yz_{max}} / \sigma_{b_{max}}$ increases as the td/T ratio decreases, emphasizing the growing significance of transverse shear stress in short-duration blast loading scenarios.

Figures 14a and 14b show that the ratio $\tau_{yz_{max}} / \sigma_{b_{max}}$ is very high during the initial stage of the response. At this early phase, the magnitude of the transverse shear stress can reach levels comparable to the bending stress (i.e., $\tau_{yz_{max}} / \sigma_{b_{max}} \approx 1$). This indicates that, in cases where the explosion occurs at close range, the glass pane may fail due to excessive shear stress. However, it is important to note that such high shear stress levels occur only for a very brief duration, on the order of microseconds.

4. CONCLUSIONS

The findings of this study confirm the significant influence of higher vibration modes on the dynamic response of glass panes subjected to close-range blast loading. The following key conclusions are drawn:

1. The finite element (FE) models have been shown to accurately simulate the short-duration dynamic response of glass panes, particularly during the critical early phase of loading. Despite minor discrepancies caused by multiple impacts in the physical experiment, the overall agreement confirms the capability and validity of the FE models for use in this application.
2. Comparative analysis between calibrated finite element (FE) simulations and single-degree-of-freedom (SDOF) models demonstrates that SDOF models can effectively estimate the maximum deflection at the centre of glass panes, provided their limitations are acknowledged.
3. Higher-mode effects were found to significantly influence the displacement, normal (bending) stress, and transverse shear stress in

glass panes, particularly under short-duration loading conditions (i.e., low td/T ratios). A correction formula was developed to improve SDOF stress estimates by accounting for the influence of higher vibration modes. This correction enhances the accuracy of SDOF predictions in short-duration blast scenarios involving glass panes supported on two sides. Furthermore, the simulations indicate that the SDOF model provides reasonably accurate results when $td/T > 0.1$.

4. At the early stage of response, very high transverse shear stress was observed, particularly near the centre of the pane. If the explosion occurs at close range, this intense shear stress, although short-lived, may cause shear failure.

ACKNOWLEDGEMENTS

The authors gratefully acknowledge Prof. Emad Gad for his valuable guidance and input during the development of the research underlying this study.

REFERENCES

1. **X. Zhang and C. Bedon**, “Vulnerability and Protection of Glass Windows and Facades under Blast: Experiments, Methods and Current Trends,” *Int. J. Struct. Glass Adv. Mater. Res.*, vol. 1, no. 2, pp. 10–23, Feb. 2017, doi: 10.3844/sgamrsp.2017.10.23.
2. **C. Bedon et al.**, “Performance of structural glass facades under extreme loads – Design methods, existing research, current issues and trends,” *Constr. Build. Mater.*, vol. 163, pp. 921–937, Feb. 2018, doi: 10.1016/j.conbuildmat.2017.12.153.
3. **H.S. Norville, Natalie Harvill, Edward J. Conrath, and Sheryll Shariat**, “Glass-Related Injuries in Oklahoma City Bombing,” *J. Perform. Constr. Facil.*, vol. 13, no. 2, pp. 50–56, May 1999.
4. **S. Das Adhikary**, “Review of Glazing and Glazing Systems under Blast Loading,” *Pract. Period. Struct. Des. Constr.*, vol. 21, no. 1, Feb. 2016, doi: 10.1061/(asce)sc.1943-5576.0000264.
5. **L. Figuli, Z. Zvaková, and C. Bedon**, “Design and Analysis of Blast Loaded Windows,” *Procedia Eng.*, vol. 192, pp. 177–182, 2017, doi: 10.1016/j.proeng.2017.06.031.
6. **J. Rudshaug, K.O. Aasen, O.S. Hopperstad, and T. Børvik**, “A physically based strength prediction model for glass,” *Int. J. Solids Struct.*, vol. 285, p. 112548, Dec. 2023, doi: 10.1016/j.ijsolstr.2023.112548.
7. **K. Fischer and I. Håring**, “SDOF response model parameters from dynamic blast loading experiments,” *Eng. Struct.*, vol. 31, no. 8, pp. 1677–1686, Aug. 2009, doi: 10.1016/j.engstruct.2009.02.040.
8. **K. Lee and J. Shin**, “Equivalent single-degree-of-freedom analysis for blast-resistant design,” *Int. J. Steel Struct.*, vol. 16, no. 4, pp. 1263–1271, Dec. 2016, doi: 10.1007/s13296-016-0073-0.
9. **S. Chen, X. Chen, G.-Q. Li, and Y. Lu**, “A theoretical study on the P-I diagram of framed monolithic glass window subjected to blast loading,” *Eng. Struct.*, vol. 150, pp. 497–510, Nov. 2017, doi: 10.1016/j.engstruct.2017.07.055.
10. AS1288, *Glass in building-Selection and installation*, Sydney, NSW., 2006.
11. **J.O. Hallquist**, *LS-DYNA Theory Manual*. Livermore, CA: Livermore Software Technology Corporation, 2006.
12. **T. Belytschko, J.I. Lin, and C.-S. Tsay**, “Explicit algorithms for the nonlinear dynamics of shells,” *Comput. Methods Appl. Mech. Eng.*, vol. 42, no. 2, Feb. 1984.
13. **J. Wei, M.S. Shetty, and L.R. Dharani**, “Failure analysis of architectural glazing subjected to blast loading,” *Eng. Fail. Anal.*, vol. 13, no. 7, pp. 1029–1043, Oct. 2006, doi: 10.1016/j.engfailanal.2005.07.010.
14. **R. Zhang, X. Zhai, X. Zhou, P. Li, and X. Zhi**, “Experimental and numerical study of annealed glass subjected to low-velocity

- impact: Simulation of windborne debris impact,” *J. Build. Eng.*, vol. 106, p. 112504, Jul. 2025, doi: 10.1016/j.job.2025.112504.
15. **M.L. Bucalem and K.J. Bathe**, “Finite Element Analysis of Shell Structures,” *Arch. Comput. Methods Eng.*, vol. 4, no. 1, pp. 3–61, 1997.
 16. **N.T.K. Lam, E.F. Gad, I. Nurhuda, and I. Calderone**, “Impact Resistance of Annealed Glass Panels,” *J. Perform. Constr. Facil.*, vol. 25, no. 5, pp. 422–432, Oct. 2011, doi: 10.1061/(asce)cf.1943-5509.0000181.
 17. **A.W.D.Q.R. Reis, R.B. Burgos, and M.F.F.D. Oliveira**, “Nonlinear Dynamic Analysis of Plates Subjected to Explosive Loads,” *Lat. Am. J. Solids Struct.*, vol. 19, no. 1, 2022, doi: 10.1590/1679-78256706.
 18. **T. Krauthammer and A. Altenberg**, “Negative phase blast effects on glass panels,” *Int. J. Impact Eng.*, vol. 24, pp. 1–17, 2000.
 19. **A. Ullah, F. Ahmad, H.-W. Jang, S.-W. Kim, and J.-W. Hong**, “Review of analytical and empirical estimations for incident blast pressure,” *KSCE J. Civ. Eng.*, vol. 21, no. 6, pp. 2211–2225, Sep. 2017, doi: 10.1007/s12205-016-1386-4.
 20. **O.R. Hansen, P. Hinze, D. Engel, and S. Davis**, “Using computational fluid dynamics (CFD) for blast wave predictions,” *J. Loss Prev. Process Ind.*, vol. 23, no. 6, pp. 885–906, Nov. 2010, doi: 10.1016/j.jlp.2010.07.005.
 21. **D. Mohotti, K. Wijesooriya, and S. Weckert**, “A simplified approach to modelling blasts in computational fluid dynamics (CFD),” *Def. Technol.*, vol. 23, pp. 19–34, May 2023, doi: 10.1016/j.dt.2022.11.006.
 22. TM5-1300, *Structures to Resist the Effects of Accidental Explosions*. Washington, DC: US Department of Army, 1990.
 23. **X. Nian, Q. Xie, X. Kong, Y. Yao, and K. Huang**, “Experimental and numerical study on protective effect of RC blast wall against air shock wave,” *Def. Technol.*, vol. 31, pp. 567–579, Jan. 2024, doi: 10.1016/j.dt.2022.11.005.
 24. **G. Randers-Pehrson and K.A. Bannister**, *Airblast Loading Model for DYNA2D and DYNA3D*. Army Research Laboratory, 1997.
 25. **M.D. Netherton and M.G. Stewart**, “The effects of explosive blast load variability on safety hazard and damage risks for monolithic window glazing,” *Int. J. Impact Eng.*, vol. 36, no. 12, pp. 1346–1354, Dec. 2009, doi: 10.1016/j.ijimpeng.2009.02.009.
 26. **I. Nurhuda, N.T.K. Lam, H. Jiang, and E.F. Gad**, “Simulation of Crack Propagation in Glass Panels Using Finite Element Analysis,” *Aust. J. Struct. Eng.*, vol. 12, no. 3, pp. 225–236, 2011.
 27. **I. Nurhuda, N.T.K. Lam, E.F. Gad, and I. Calderone**, “Estimation of strengths in large annealed glass panels,” *Int. J. Solids Struct.*, vol. 47, no. 18–19, pp. 2591–2599, 2010.

СПИСОК ЛИТЕРАТУРЫ

1. **X. Zhang and C. Bedon**, “Vulnerability and Protection of Glass Windows and Facades under Blast: Experiments, Methods and Current Trends,” *Int. J. Struct. Glass Adv. Mater. Res.*, vol. 1, no. 2, pp. 10–23, Feb. 2017, doi: 10.3844/sgamrsp.2017.10.23.
2. **C. Bedon et al.**, “Performance of structural glass facades under extreme loads – Design methods, existing research, current issues and trends,” *Constr. Build. Mater.*, vol. 163, pp. 921–937, Feb. 2018, doi: 10.1016/j.conbuildmat.2017.12.153.
3. **H.S. Norville, Natalie Harvill, Edward J. Conrath, and Sheryll Shariat**, “Glass-Related Injuries in Oklahoma City Bombing,” *J. Perform. Constr. Facil.*, vol. 13, no. 2, pp. 50–56, May 1999.
4. **S. Das Adhikary**, “Review of Glazing and Glazing Systems under Blast Loading,” *Pract. Period. Struct. Des. Constr.*, vol. 21, no. 1, Feb. 2016, doi: 10.1061/(asce)sc.1943-5576.0000264.
5. **L. Figuli, Z. Zvaková, and C. Bedon**, “Design and Analysis of Blast Loaded Windows,” *Procedia Eng.*, vol. 192, pp.

- 177–182, 2017, doi: 10.1016/j.proeng.2017.06.031.
6. **J. Rudshaug, K.O. Aasen, O.S. Hopperstad, and T. Børvik**, “A physically based strength prediction model for glass,” *Int. J. Solids Struct.*, vol. 285, p. 112548, Dec. 2023, doi: 10.1016/j.ijsolstr.2023.112548.
 7. **K. Fischer and I. Häring**, “SDOF response model parameters from dynamic blast loading experiments,” *Eng. Struct.*, vol. 31, no. 8, pp. 1677–1686, Aug. 2009, doi: 10.1016/j.engstruct.2009.02.040.
 8. **K. Lee and J. Shin**, “Equivalent single-degree-of-freedom analysis for blast-resistant design,” *Int. J. Steel Struct.*, vol. 16, no. 4, pp. 1263–1271, Dec. 2016, doi: 10.1007/s13296-016-0073-0.
 9. **S. Chen, X. Chen, G.-Q. Li, and Y. Lu**, “A theoretical study on the P-I diagram of framed monolithic glass window subjected to blast loading,” *Eng. Struct.*, vol. 150, pp. 497–510, Nov. 2017, doi: 10.1016/j.engstruct.2017.07.055.
 10. AS1288, *Glass in building-Selection and installation*, Sydney, NSW., 2006.
 11. **J.O. Hallquist**, *LS-DYNA Theory Manual*. Livermore, CA: Livermore Software Technology Corporation, 2006.
 12. **T. Belytschko, J.I. Lin, and C.-S. Tsay**, “Explicit algorithms for the nonlinear dynamics of shells,” *Comput. Methods Appl. Mech. Eng.*, vol. 42, no. 2, Feb. 1984.
 13. **J. Wei, M.S. Shetty, and L.R. Dharani**, “Failure analysis of architectural glazing subjected to blast loading,” *Eng. Fail. Anal.*, vol. 13, no. 7, pp. 1029–1043, Oct. 2006, doi: 10.1016/j.engfailanal.2005.07.010.
 14. **R. Zhang, X. Zhai, X. Zhou, P. Li, and X. Zhi**, “Experimental and numerical study of annealed glass subjected to low-velocity impact: Simulation of windborne debris impact,” *J. Build. Eng.*, vol. 106, p. 112504, Jul. 2025, doi: 10.1016/j.jobbe.2025.112504.
 15. **M.L. Bucalem and K.J. Bathe**, “Finite Element Analysis of Shell Structures,” *Arch. Comput. Methods Eng.*, vol. 4, no. 1, pp. 3–61, 1997.
 16. **N.T.K. Lam, E.F. Gad, I. Nurhuda, and I. Calderone**, “Impact Resistance of Annealed Glass Panels,” *J. Perform. Constr. Facil.*, vol. 25, no. 5, pp. 422–432, Oct. 2011, doi: 10.1061/(asce)cf.1943-5509.0000181.
 17. **A.W.D.Q.R. Reis, R.B. Burgos, and M.F.F.D. Oliveira**, “Nonlinear Dynamic Analysis of Plates Subjected to Explosive Loads,” *Lat. Am. J. Solids Struct.*, vol. 19, no. 1, 2022, doi: 10.1590/1679-78256706.
 18. **T. Krauthammer and A. Altenberg**, “Negative phase blast effects on glass panels,” *Int. J. Impact Eng.*, vol. 24, pp. 1–17, 2000.
 19. **A. Ullah, F. Ahmad, H.-W. Jang, S.-W. Kim, and J.-W. Hong**, “Review of analytical and empirical estimations for incident blast pressure,” *KSCE J. Civ. Eng.*, vol. 21, no. 6, pp. 2211–2225, Sep. 2017, doi: 10.1007/s12205-016-1386-4.
 20. **O.R. Hansen, P. Hinze, D. Engel, and S. Davis**, “Using computational fluid dynamics (CFD) for blast wave predictions,” *J. Loss Prev. Process Ind.*, vol. 23, no. 6, pp. 885–906, Nov. 2010, doi: 10.1016/j.jlp.2010.07.005.
 21. **D. Mohotti, K. Wijesooriya, and S. Weckert**, “A simplified approach to modelling blasts in computational fluid dynamics (CFD),” *Def. Technol.*, vol. 23, pp. 19–34, May 2023, doi: 10.1016/j.dt.2022.11.006.
 22. TM5-1300, *Structures to Resist the Effects of Accidental Explosions*. Washington, DC: US Department of Army, 1990.
 23. **X. Nian, Q. Xie, X. Kong, Y. Yao, and K. Huang**, “Experimental and numerical study on protective effect of RC blast wall against air shock wave,” *Def. Technol.*, vol. 31, pp. 567–579, Jan. 2024, doi: 10.1016/j.dt.2022.11.005.
 24. **G. Randers-Pehrson and K.A. Bannister**, *Airblast Loading Model for DYNA2D and DYNA3D*. Army Research Laboratory, 1997.
 25. **M.D. Netherton and M.G. Stewart**, “The effects of explosive blast load variability on

- safety hazard and damage risks for monolithic window glazing,” *Int. J. Impact Eng.*, vol. 36, no. 12, pp. 1346–1354, Dec. 2009, doi: 10.1016/j.ijimpeng.2009.02.009.
26. **I. Nurhuda, N.T.K. Lam, H. Jiang, and E.F. Gad**, “Simulation of Crack Propagation in Glass Panels Using Finite Element Analysis,” *Aust. J. Struct. Eng.*, vol. 12, no. 3, pp. 225–236, 2011.
27. **I. Nurhuda, N.T.K. Lam, E.F. Gad, and I. Calderone**, “Estimation of strengths in large annealed glass panels,” *Int. J. Solids Struct.*, vol. 47, no. 18–19, pp. 2591–2599, 2010.

Ilham Nurhuda, Dr., Senior Lecturer, Department of Civil Engineering, Diponegoro University (Undip). Jl. Prof. Soedarto, S.H., Tembalang, Semarang, 50275, Indonesia. E-mail: ilham@live.undip.ac.id.

Илхам Нурхуда, д.т.н., старший преподаватель, кафедра гражданского строительства, Университет Дипонегоро (Undip). Ул. Проф. Соедарто, С.Н., Тембаланг, Семаранг, 50275, Индонезия. E-mail: ilham@live.undip.ac.id.

Nelson T.K. Lam, Professor, Department of Infrastructure Engineering, The University of Melbourne (UniMelb), Grattan Street, Parkville, Victoria, 3010, Australia. E-mail: ntkl@unimelb.edu.au

Нельсон Т.К. Лам, д.т.н., профессор, кафедра инженерии инфраструктуры, Мельбурнский университет (UniMelb), Граттан-стрит, Парквилл, Виктория, 3010, Австралия. E-mail: ntkl@unimelb.edu.au